Research Article | Vol. 8, No. 10 | 1 Oct 2017 | BIOMEDICAL OPTICS EXPRESS 4438
Biomedical Optics EXPRESS

Flow-through micro-capillary refractive index sensor based on T/R spectral shift monitoring

GIULIA RIGAMONTI,[1] MARCO GUARDAMAGNA,[1] VALENTINA BELLO,[1] STEFANIA MARCONI,[2] FERDINANDO AURICCHIO,[2] AND SABINA MERLO[1,*]

[1]*Dipartimento di Ingegneria Industriale e dell'Informazione, University of Pavia, 27100, Pavia, Italy*
[2]*Dipartimento di Ingegneria Civile e Architettura, University of Pavia, 27100, Pavia, Italy*
[*]*sabina.merlo@unipv.it*

Abstract: We present a flow-through refractive index sensor for measuring the concentration of glucose solutions based on the application of rectangular glass micro-capillaries, with channel depth of 50 µm and 30 µm. A custom designed and 3D printed polymeric shell protects the tiny capillaries, ensuring an easier handling and interconnection with the macro-fluidic path. By illuminating the capillary with broadband radiation centered at λ~1.55 µm, both the transmitted (T) and reflected (R) optical spectrum from the capillary are detected with an optical spectrum analyzer, exploiting an all-fiber setup. Monitoring the spectral shift of the ratio T/R in response to increasing concentration of glucose solutions in water we have obtained sensitivities up to 530.9 nm/RIU and limit of detection in the range of 10^{-5}-10^{-4} RIU. Experimental results are in agreement with the theoretically predicted principle of operation. After the demonstration of amplitude detection at a single wavelength, we finally discuss the impact of the capillary parameters on the sensitivity.

OCIS codes: (120.0280) Remote sensing and sensors; (120.4640) Optical instruments; (230.3990) Micro-optical devices; (280.1415) Biological sensing and sensors; (280.1545) Chemical analysis; (280.4788) Optical sensing and sensors; (300.6170) Spectra.

References and links

1. H. K. Hunt and A. M. Armani, "Label-free biological and chemical sensors," Nanoscale **2**(9), 1544–1559 (2010).
2. N. M. M. Pires, T. Dong, U. Hanke, and N. Hoivik, "Recent developments in optical detection technologies in lab-on-a-chip devices for biosensing applications," Sensors (Basel) **14**(8), 15458–15479 (2014).
3. A. A. P. Trichet, J. Foster, N. E. Omori, D. James, P. R. Dolan, G. M. Hughes, C. Vallance, and J. M. Smith, "Open-access optical microcavities for lab-on-a-chip refractive index sensing," Lab Chip **14**(21), 4244–4249 (2014).
4. V. Passaro, B. Troia, M. La Notte, and F. De Leonardis, "Photonic resonant microcavities for chemical and biochemical sensing," RSC Advances **3**(1), 25–44 (2013).
5. M. Huang, A. A. Yanik, T. Y. Chang, and H. Altug, "Sub-wavelength nanofluidics in photonic crystal sensors," Opt. Express **17**(26), 24224–24233 (2009).
6. E. Chow, A. Grot, L. W. Mirkarimi, M. Sigalas, and G. Girolami, "Ultracompact biochemical sensor built with two-dimensional photonic crystal microcavity," Opt. Lett. **29**(10), 1093–1095 (2004).
7. G. Barillaro, S. Merlo, S. Surdo, L. M. Strambini, and F. Carpignano, "Integrated optofluidic microsystem based on vertical high-order one-dimensional silicon photonic crystals," Microfluid. Nanofluidics **12**(1), 545–552 (2012).
8. S. Surdo, S. Merlo, F. Carpignano, L. M. Strambini, C. Trono, A. Giannetti, F. Baldini, and G. Barillaro, "Optofluidic microsystems with integrated vertical one-dimensional photonic crystals for chemical analysis," Lab Chip **12**(21), 4403–4415 (2012).
9. S. Surdo, F. Carpignano, L. M. Strambini, S. Merlo, and G. Barillaro, "Capillarity-driven (self-powered) one-dimensional photonic crystals for refractometry and (bio)sensing applications," RSC Advances **4**(94), 51935–51941 (2014).
10. C. A. Barrios, M. J. Bañuls, V. González-Pedro, K. B. Gylfason, B. Sánchez, A. Griol, A. Maquieira, H. Sohlström, M. Holgado, and R. Casquel, "Label-free optical biosensing with slot-waveguides," Opt. Lett. **33**(7), 708–710 (2008).
11. H. Li and X. Fan, "Characterization of sensing capability of optofluidic ring resonator biosensors," Appl. Phys. Lett. **97**(1), 011105 (2010).
12. G. Testa, Y. Huang, P. M. Sarro, L. Zeni, and R. Bernini, "Integrated silicon optofluidic ring resonator," Appl. Phys. Lett. **97**(13), 131110 (2010).
13. C. Ciminelli, C. M. Campanella, F. Dell'Olio, C. E. Campanella, and M. N. Armenise, "Label-free optical

#297571 https://doi.org/10.1364/BOE.8.004438
Journal © 2017 Received 13 Jun 2017; revised 25 Jul 2017; accepted 31 Jul 2017; published 11 Sep 2017

Biomedical Optics EXPRESS

resonant sensors for biochemical applications," Prog. Quantum Electron. **37**(2), 51–107 (2013).
14. K. De Vos, I. Bartolozzi, E. Schacht, P. Bienstman, and R. Baets, "Silicon-on-Insulator microring resonator for sensitive and label-free biosensing," Opt. Express **15**(12), 7610–7615 (2007).
15. J. H. Wade and R. C. Bailey, "Applications of optical microcavity resonators in analytical chemistry," Annu. Rev. Anal. Chem. (Palo Alto, Calif.) **9**(1), 1–25 (2016).
16. M. R. Foreman, J. D. Swaim, and F. Vollmer, "Whispering gallery mode sensors," Adv. Opt. Photonics **7**(2), 168–240 (2015).
17. W. Morrish, P. West, N. Orlando, E. Klantsataya, K. Gardner, S. Lane, R. Decorby, A. François, and A. Meldrum, "Refractometric Micro-Sensor Using a Mirrored Capillary Resonator," Opt. Express **24**(22), 24959–24970 (2016).
18. M. Evander and M. Tenje, "Microfluidic PMMA interfaces for rectangular glass capillaries," J. Micromech. Microeng. **24**(2), 027003 (2014).
19. S. Calixto, M. Rosete-Aguilar, D. Monzon-Hernandez, and V. P. Minkovich, "Capillary refractometer integrated in a microfluidic configuration," Appl. Opt. **47**(6), 843–848 (2008).
20. T. Tsuda, J. V. Sweedler, and R. N. Zare, "Rectangular capillaries for capillary zone electrophoresis," Anal. Chem. **62**(19), 2149–2152 (1990).
21. B. Hammarström, M. Evander, H. Barbeau, M. Bruzelius, J. Larsson, T. Laurell, and J. Nilsson, "Non-contact acoustic cell trapping in disposable glass capillaries," Lab Chip **10**(17), 2251–2257 (2010).
22. M. Born and E. Wolf, *Principles of Optics* (Pergamon Press, 1986).
23. S. J. Orfanidis, *Electromagnetic Waves and Antennas* (2008), Chap. 6.
24. F. Carpignano, G. Rigamonti, T. Migliazza, and S. Merlo, "Refractive index sensing in rectangular glass micro-capillaries by spectral reflectivity measurments," IEEE J. Sel. Top. Quantum Electron. **22**(3), 1–9 (2015).
25. Y. Zhou, Y. Hu, N. Zeng, Y. Ji, X. Dai, P. Li, H. Ma, and Y. He, "Noninvasive monitoring of Pirenoxine Sodium concentration in aqueous humor based on dual-wavelength iris imaging technique," Biomed. Opt. Express **2**(2), 231–242 (2011).
26. R. Cheng and L. Xia, "Interrogation of weak Bragg grating sensors based on dual-wavelength differential detection," Opt. Lett. **41**(22), 5254–5257 (2016).
27. U. S. Raikar, V. K. Kulkarni, A. S. Lalasangi, K. Madhav, and S. Asokan, "Etched fiber Bragg grating as ethanol solution concentration sensor," Adv. Mater. **1**(4), 149–151 (2007).
28. W. Zhang, D. Webb, and G. Peng, "Polymer optical fiber Bragg grating acting as an intrinsic biochemical concentration sensor," Opt. Lett. **37**(8), 1370–1372 (2012).
29. M. S. Kwon and W. H. Steier, "Microring-resonator-based sensor measuring both the concentration and temperature of a solution," Opt. Express **16**(13), 9372–9377 (2008).
30. *Datasheet "BOROFLOAT 33 glass - Optical Properties", SCHOTT North America Inc.,* https://refractiveindex.info/?shelf=glass&book=SCHOTT-multipurpose&page=BOROFLOAT33
31. P. L. Gourley, "Biocavity laser for high-speed cell and tumour biology," J. Phys. D Appl. Phys. **36**(14), R228–R239 (2003).
32. T. Tumolo, L. Angnes, and M. S. Baptista, "Determination of the refractive index increment (dn/dc) of molecule and macromolecule solutions by surface plasmon resonance," Anal. Biochem. **333**(2), 273–279 (2004).
33. Y. Temiz, R. D. Lovchik, G. V. Kaigala, and E. Delamarche, "Lab-on-a-chip devices: how to close and plug the lab?" Microelectron. Eng. **132**, 156–175 (2015).
34. I. M. White and X. Fan, "On the performance quantification of resonant refractive index sensors," Opt. Express **16**(2), 1020–1028 (2008).
35. F. Carpignano, G. Rigamonti, G. Mazzini, and S. Merlo, "Low-coherence reflectometry for refractive index measurements of cells in micro-capillaries," Sensors **16**(10), 1670 (2016).
36. F. Carpignano, G. Rigamonti, and S. Merlo, "Characterization of rectangular glass microcapillaries by low-coherence reflectometry," IEEE Photonics Technol. Lett. **27**(10), 1064–1067 (2015).
37. K. Zirk and H. Poetzschke, "A refractometry-based glucose analysis of body fluids," Med. Eng. Phys. **29**(4), 449–458 (2007).

1. Introduction

In the last few years, increasing attention has been paid to optical sensors for the detection of fluid refractive index (RI) and/or of solution concentration. Label-free sensing is object of great interest, since, with respect to methods based on exogenous markers, it is safer, less invasive and usually cheaper [1,2]. Optical read-out is undoubtedly a very fascinating solution among detection methods, as it allows remote sensing of the investigated parameters, being thus minimally invasive, while miniaturization enables testing with ultra-low quantities of materials, both important factors particularly in the fields of biological, biochemical and biomedical analyses [2]. Various types of sensors that respond to the mentioned requirements have been lately investigated, based on resonant micro-cavities [1,3,4], photonics crystals [5–9], ring resonators [10–15], or whispering gallery modes [16], just to cite a few of them. However, there is still the need of demonstrating the functionality of simple and low-cost

Biomedical Optics EXPRESS

devices to be used as core elements of micro-opto-fluidic sensors combined with suitable readout methods. Glass micro-capillaries, available in different sizes and shapes, may represent a convenient response to this necessity as they are off-the-shelf disposable devices easily filled with small volumes and in principle suitable for assembling fluidic systems. Morrish *et al.* [17], for example, used mirrored round micro-capillaries as gas and liquid sensors. Evander *et al.* [18] designed and fabricated a PMMA fluidic interface for rectangular micro-capillaries and performed non-contact trapping of polystyrene beads as an example of application in the field of acoustophoresis. Calixto *et al*. [19] used a round capillary encapsulated with two fibers as liquid RI detector. Tsuda *et al.* [20] employed rectangular micro-capillaries to perform zone electrophoresis, while Hammarstrom *et al.* [21] exploited rectangular glass capillaries as elements for trapping and dispensing red blood cells. Rectangular cross-section capillaries, in particular, are better suited for optical read-out methods, thanks to their flat surface that reduces scattering and optical distortions usually occurring with circular capillaries [20]. Moreover, they resemble an optical resonator, composed by three flat parallel slabs, i.e., two glass walls and the internal channel [22,23].

In a previous work, we demonstrated refractive index sensing of fluids, collected in rectangular micro-capillaries, by spectral reflectivity measurements in the near infrared [24]. When capillaries are illuminated orthogonally to their flat long side with broadband radiation, the reflected power spectrum exhibits wavelength regions where the intensity is very high followed by regions of low intensity. A good agreement with theoretically expected spectra was already demonstrated in [24]. As the wavelength positions of the reflectivity minima depend on the refractive index of the fluid, the refractive index change with respect to a reference fluid was recovered by monitoring the shift of the reflected power spectrum. This method of RI detection requires a thorough spectral analyses or, eventually, intensity monitoring but at least at two different wavelengths [13, 24–26].

Interesting features of rectangular glass micro-capillaries are their transparency and their symmetric structure that allow collection not only of the reflected light spectrum but also of the transmitted radiation. In this work, we have thus extended the model (for further detail, see the Appendix section) to calculate spectral reflectivity and transmissivity using Fresnel equations for retrieving the T/R spectral ratio. We have observed, both theoretically and experimentally, that reflected and transmitted spectral signals exhibit large intensity variations as a function of the wavelength and spectral regions of reflectivity maxima correspond to transmissivity minima (and vice versa). Acquisition of both reflected (R) and transmitted (T) spectra represents undoubtedly an advantage with respect to standard reflectometry, since the evaluation of the T/R ratio allows to compensate for intensity fluctuations of the read-out source, with no need of an additional monitoring system of the emitted optical power.

The optical read-out method proposed in this work for refractive index sensing of fluids flowing in the capillary channel is based on the observation that the T/R ratio shifts toward longer wavelengths for increasing values of the refractive index of the filling fluid. Moreover, as T and R are complementary, taking their ratio improves the output signal dynamic range and paves the way for reliably translating spectral shifts due to RI changes into amplitude variations at a single wavelength. The rectangular glass micro-capillary is thus a good candidate as core element for the realization of a flow-through refractive index sensor based on optical T/R detection. In this paper, we are presenting and comparing the performances of three standard types of rectangular glass micro-capillaries (commercially available), featuring different combinations of wall thickness and channel depth. We have investigated micro-capillaries characterized by a nominal channel depth of 50 µm sandwiched between either 50-µm-thick or 35-µm-thick walls and even thinner micro-capillaries with 30-µm-deep channel and 30-µm-thick walls. All of them have been applied for the demonstration of flow-through chemical sensing for RI detection of water/glucose solutions, based on T/R detection. Both theoretical and experimental results are presented and compared.

Biomedical Optics EXPRESS

With the purposes of protecting the thin glass micro-structure and of more easily interfacing the capillary micro-channel to an external fluidic path, a custom polymeric shell with butterfly shape has been designed, 3D printed and used in the optical testing of all capillaries. By means of infrared broadband radiation centered at a wavelength of 1550 nm, we have achieved remote, non-contact read-out of the concentration of glucose solutions. Filling of the micro-channel is attained just by capillary action whereas a peristaltic pump helps discarding the sample after test. By monitoring the wavelength shift of the T/R peaks induced by solutions of glucose in water at different concentrations, we have demonstrated sensitivities in the range from 258.0 nm/RIU up to 530.9 nm/RIU and limit of detection (LOD) in the range of 10^{-5}-10^{-4} RIU. These results are comparable with data reported in the literature [27–29] for more complex devices, sometimes attainable only with expensive and lengthy microfabrication techniques. After demonstration of amplitude detection at a single wavelength as an alternative to spectral shift monitoring, a discussion relative to the impact of the capillary dimensions on the sensitivity is finally reported.

2. Principle of operation

A rectangular micro-capillary, shown in Fig. 1, when illuminated orthogonally with respect to its long flat surface, can be viewed as an optical resonator composed by three adjacent layers, namely, the front glass wall, the internal channel, and the back wall. The traveling light crosses four different interfaces, i.e., for an empty capillary, two air-glass interfaces (corresponding to the left side of the front and back walls in Fig. 1) and two glass-air interfaces (corresponding to the right side of the walls in Fig. 1).

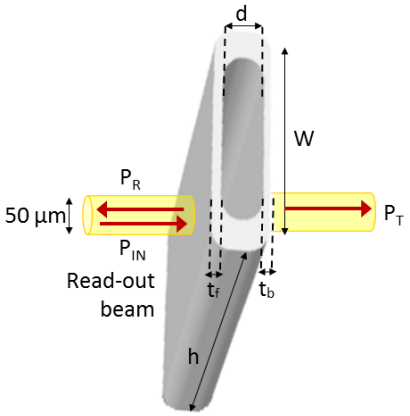

Fig. 1. 3D sketch of a glass rectangular micro-capillary.

The capillary can be considered as a multilayer structure composed by materials with different RI and thicknesses along a single axis (1-D structure). If the light beam diameter is significantly smaller with respect to the length and width of the shined face, a simple approach based on planar wave propagation can be used to calculate the reflectivity and transmissivity through the device. Following investigations that are reported in a previous work relative to spectral reflectivity of rectangular glass micro-capillaries [24], in this work we have completed the model (for further details, see the Appendix) for calculating the spectral behavior of optical power reflectivity R and transmissivity T and for retrieving the T/R ratio. Briefly, transmission and reflection coefficients for the electric field traveling with normal incidence though the device have been calculated recursively through Matlab software, and then from the superposition of all contributions, the optical power reflectivity and transmissivity have been obtained. Glass RI dependence on the wavelength has been taken into account through interpolation of data obtained from the literature (BOROFLOAT 33 Schott Glass) [30], whereas wavelength dependence of the refractive index of the filling

Biomedical Optics EXPRESS

fluid has been neglected in the simulations. Figure 2 shows the theoretical spectra of optical power reflectivity and transmissivity, calculated with the procedure described in the Appendix section, relative to a symmetric capillary with channel depth d and walls thickness t_f (front wall) and t_b (back wall) all equal to 50 μm, and refractive index of the medium contained in the inner channel equal to that of water (n_{fluid} = 1.3154), on a wavelength range from 1510 nm to 1570 nm. It is evident that the wavelength positions of transmissivity maxima correspond to positions of reflectivity minima.

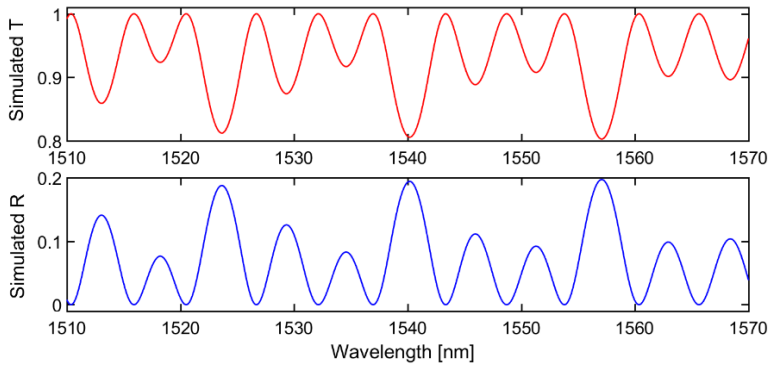

Fig. 2. Theoretical spectra obtained by using Fresnel equations for modeling the optical behavior of a capillary with $d = t_b = t_f = 50$ μm and $n_{fluid} = 1.3154$. Upper red trace: optical power transmissivity; Lower blue trace: optical power reflectivity. A moving average has been applied to mimic the limited resolution bandwidth of the Optical Spectrum Analyzer employed in the following experimental verification.

Figure 3(a) shows T/R spectra, calculated as the ratio between theoretical transmissivity and reflectivity, attained for different RI values of the medium filling the channel. A clear shift toward longer wavelength is observable as the channel RI increases. The Δλ highlighted in the figure is the distance, in terms of wavelength, between two consecutive maxima of the same spectrum; it is an important parameter of devices with multiple optical resonances since it gives the largest shift that can be followed without ambiguity, limiting therefore the largest refractive index variation that can be detected without ambiguity. It should be noticed as the spectrum does not rigidly shift but peaks facing a larger Δλ undergo a wider translation, compared to others, given the same RI change.

The spectral dependence of T and R, as well as of T/R, can be interpreted as resulting from the superposition of the contributions of different cavities or Fabry-Perot etalons. Each resonance peak is the result of contributions coming from different interfaces. To highlight the contribution given by each cavity, we have calculated the Fast Fourier Transform (FFT) of the theoretical T/R spectra (in the wavelength range 1400-1600 nm) relative to a 50-μm capillary filled with water (n_{fluid} = 1.3154 RIU). The result is shown in Fig. 3(b): three main peaks can be easily recognized occurring at $1/\lambda_1 = 65\ \mu m^{-1}$, $1/\lambda_2 = 125\ \mu m^{-1}$, $1/\lambda_3 = 190\ \mu m^{-1}$.

Biomedical Optics EXPRESS

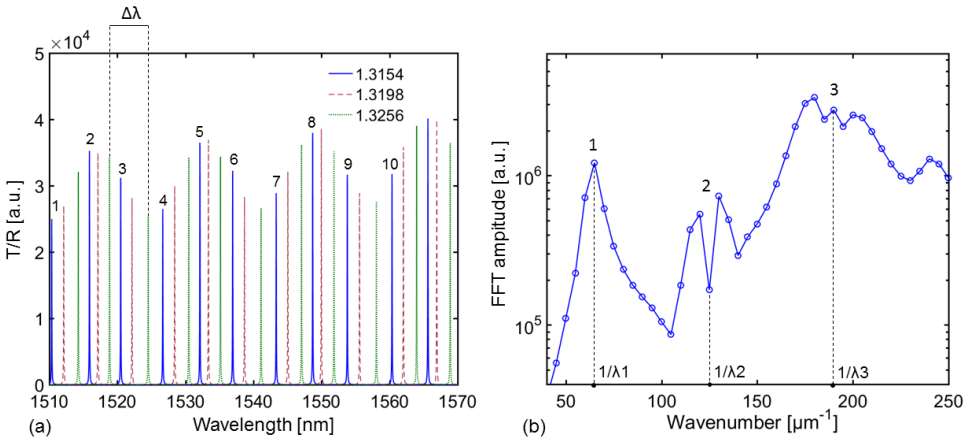

Fig. 3. (a) Calculated T/R spectra from theoretical analysis performed for a capillary with $d = t_b = t_f = 50$ μm and increasing n_{fluid} values. Blue trace: $n_{fluid} = 1.3154$ RIU; red dashed trace: $n_{fluid} = 1.3198$ RIU; green dotted trace: $n_{fluid} = 1.3256$ RIU. Δλ: distance in wavelength between two consecutive peaks of the same spectrum. (b) Fast Fourier Transform of the theoretical T/R spectrum reported in (a), relative to the capillary filled with water ($n_{fluid} = 1.3154$ RIU), blue trace, as a function of the wavenumber 1/λ. The y axis is expressed in logarithmic scale for better visualization.

For a Fabry-Perot cavity, it is well known that the Free Spectral Range (FSR) is given by $FSR = \lambda^2/[2 \bullet OP]$, where OP is the Optical Path of the considered cavity and λ the wavelength position of the resonance. In the case of the capillary, the cavity formed by a single wall has an optical path given by $OP_{wall} = n_{glass} \bullet t_b$ or $OP_{wall} = n_{glass} \bullet t_f$ (assuming $n_{glass} = 1.4561$ RIU), whereas for the cavity corresponding to the channel we get $OP_{channel} = n_{fluid} \bullet d$. Another cavity is due to the whole capillary, thus with $OP_{capillary} = n_{fluid} \bullet d + n_{glass} \bullet (t_f + t_b)$ and, finally, there is also a component due to the combined cavity formed by the channel plus one wall with $OP_{wall + channel} = n_{glass} \bullet t_f + n_{fluid} \bullet d$ or $OP_{wall + channel} = n_{glass} \bullet t_b + n_{fluid} \bullet d$. It can be easily calculated that, when a fluid is filling the channel, $1/\lambda_1 \approx 1/FSR_{wall} \approx 1/FSR_{channel}$, $1/\lambda_2 \approx 1/FSR_{wall + channel}$ and $1/\lambda_3 \approx 1/FSR_{capillary}$. The Fourier spectrum is broader at $1/\lambda_2$ and $1/\lambda_3$ because the mode spacing does not remain uniform in wavelength units. This analysis gives a better insight on the contribution of the capillary structure to the T/R spectrum.

As we are interested in exploiting the shift of the T/R spectrum as a function of the filling fluid refractive index for sensing purposes, from the simulated spectra we have extracted the wavelength positions of the T/R maxima for different fluid RIs. Figure 4(a) reports the theoretical calibration curves, obtained by varying the fluid RI from 1.3154 RIU to 1.3299 RIU, that consist in the wavelength position of the T/R maxima as a function the channel RI. The selected RI values correspond to the RI of glucose solutions in water with concentrations from 0 to 10% [weight/Volume, w/V] that will be used in the experiments. The RI values of Glucose solutions have been obtained from the equation $n = n_0 + \alpha \bullet C$ [31], where n_0 is the RI of the solvent, in our case water (thus, $n_0 = 1.3154$ RIU), C is the concentration of the solute and $\alpha = dn/dC$ is the RI increment, specific for each solute. For glucose, $\alpha = 0.145$ cm^3/g [32]. Sensitivities, defined as $S = d\lambda_{max}/dn_{fluid}$, reported on the right side of Fig. 4(a) for each curve, are obtained through linear fitting of the data with least square method. It can be noticed as different resonances, or maxima, result in different sensitivity values. Rectangular glass capillaries are commercially available in a wide range of dimensions and combinations of walls thickness and channel depth. To investigate the dependence of the device performance (for RI sensing) on its dimensions, we have calculated with numerical simulations the T/R spectra for capillaries with the same channel depth, set equal to 50 μm, and increasing glass walls, in a range from 20 μm up to 110 μm.

Biomedical Optics EXPRESS

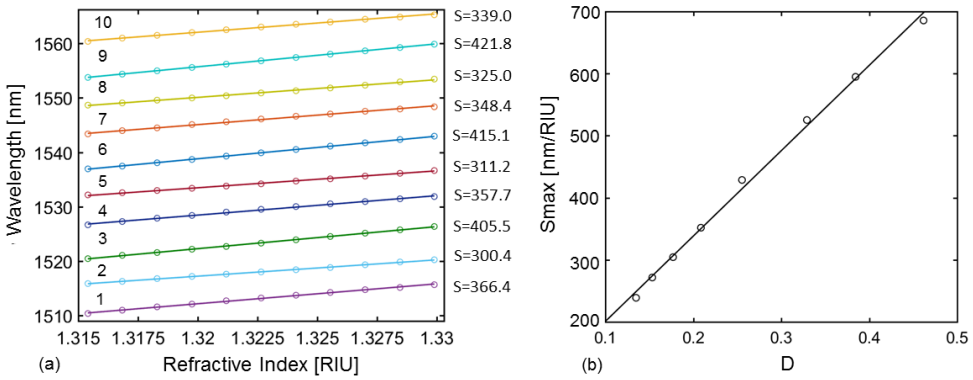

Fig. 4. (a) Calibration curves obtained from theoretical T/R spectra for a capillary with $d = t_b = t_f = 50$ µm and n_{fluid} in the range of 1.3154-1.3299 RIU. Numerical values on the right side represent the sensitivities obtained through linear fitting of the data, reported in nm/RIU units. The numbers reported near each fitting line recall the peak labels highlighted in Fig. 3(a). (b) Best sensitivity values obtained from T/R theoretical spectra calculated for channel depth d = 50 µm and different wall thicknesses (from 20 µm up to 110 µm) as a function of $D = d/[d + n_{glass} \bullet (t_f + t_b)]$, where t_f is the front wall thickness and t_b the back wall thickness.

For each combination of geometric parameters, we have also investigated the spectral shift as a function of the RI medium filling the channel. As mentioned before, the collected spectrum is a superimposition of contributions coming from different cavities, but only the channel is affected by fluid RI changes. Intuitively, one would expect that the deeper is the channel compared to the total capillary optical thickness, the higher should be the relative sensitivity. We have thus introduced a parameter $D = d / [d + n_{glass} \bullet (t_f + t_b)]$, where n_{glass} is the glass RI and $n_{glass} \bullet t$ represents the optical path travelled by light when crossing the glass walls. We have then investigated the relationship between the best RI sensitivity S_{max} numerically obtained for each considered capillary structure (in the wavelength range 1400-1600 nm) and its characterizing D. The result reported in Fig. 4(b) shows that larger values of S_{max} correspond to higher values of D. The relationship is approximately linear, with a correlation coefficient R = 0.9970 between S_{max} and D. Data reported in Fig. 4(b) have been obtained considering in the simulations $t_f = t_b$ and both equal to 20 µm, 27.5 µm, 35 µm, 50 µm, 65 µm, 80 µm, 95 µm, 110 µm, resulting in D equal, respectively, to 0.462, 0.384, 0.329, 0.256, 0.209, 0.178, 0.153, 0.135 (with $n_{glass} = 1.4561$ RIU).

3. Experimental configuration

3.1 Rectangular glass micro-capillaries

Rectangle miniature hollow borosilicate glass tubings (Vitrotubes, VitroCom, New Jersey, USA) shown in Fig. 1 were used as core micro-capillary of the proposed micro-fluidic system. We experimentally investigated devices with channel depth $d = 50$ µm, side width W = 500 µm and wall thickness either $t_f = t_b = 35$ µm or $t_f = t_b = 50$ µm, as well as devices with $t_f = t_b = d = 30$ µm and width W = 300 µm (all nominal values). All capillaries were 5 cm long. The manufacturer ensured in standard products a tolerance of 10% for the channel depth and for the side width, and 20% for the wall thicknesses t. The system response to glucose/water solutions at different concentrations was obtained by dipping one tip of the capillary into an Eppendorf tube containing the solutions. The liquid samples were instantly collected into the channel by capillary action, whereas a peristaltic pump was used to discard the fluid after the measurements.

Biomedical Optics EXPRESS

3.2 3D printed polymeric support

Despite micro-fluidic devices are nowadays widely diffused in many applications, the connection of miniaturized systems with the external world remains still challenging [33]. We developed a proper solution to facilitate support and integration of the micro-capillary in the experimental set up, by using 3D printing technology. The support structure was designed with a CAD software (SolidWorks - Dassault Systèmes) and it is composed by four parts to be assembled (Fig. 5). The main structure holds the micro-capillary in its central semicircular channel, whereas two rectangular handles with holes allow fixing the whole device in the experimental set up. The main structure is divided into two symmetric halves to enable the placement of the micro-capillary and it can be fastened by means of two threaded caps of different length (Fig. 5(a)-5(b)). Indeed, the structure presents two endings of different shape: the shortest ending allows the fluidic feeding of the micro-capillary, while the most extended one allows the connection with the external fluidic path. A window placed in the middle of the structure ensures a clear path for the readout optical beam. The four parts are exported as Standard Triangulation Language (STL) format.

STL models were printed using a Form2 (Formlabs) printer, based on stereolithographic technology: a clear methacrylate photopolymer resin (FLGPCL03), printed at a layer thickness of 25 μm, was found suitable for this application.

Due to the brittleness and the narrow section of the micro-capillary we endowed the structure with 4 silicon bearings fitting the inner channel of the support to protect the micro-capillary from being damaged by the contact with the rigid walls (Fig. 5(a)). Bearings were created using a 3D printed mold in which to pour a bi-component silicon mixture (Sylgard 184 – Dow Corning).

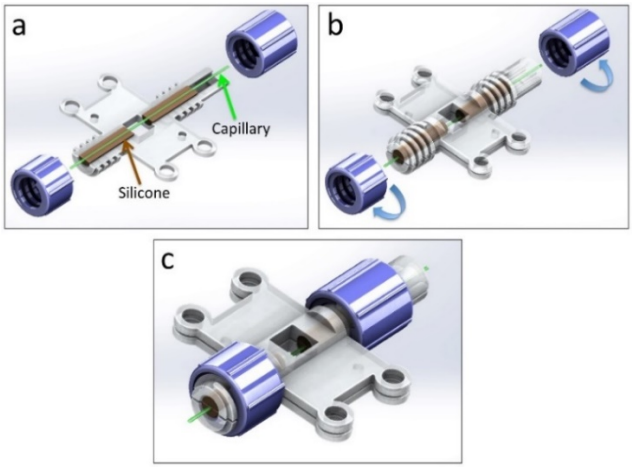

Fig. 5. 3D-printed polymeric support.

3.3 Experimental setup

Figure 6 shows the block diagram of the instrumental configuration used for spectral measurements. Readout radiation in the near-infrared range was provided by a Superluminescent Light Emitting Diode (SLED) source with peak emission wavelength λ_c ~1549 nm, Full Width at Half Maximum (FWHM) bandwidth of 57 nm and optical power coupled in standard single-mode optical fibers of approximately 1.8 mW when driven by a pumping current of I = 180 mA at a temperature of 20 °C. The SLED was protected from unwanted optical feedback with a fiber-pigtailed optical isolator. Radiation was carried toward the capillary under test through a 2x2 fiber coupler with 50:50 splitting ratio and flat spectral response, in the wavelength region of interest.

Biomedical Optics EXPRESS

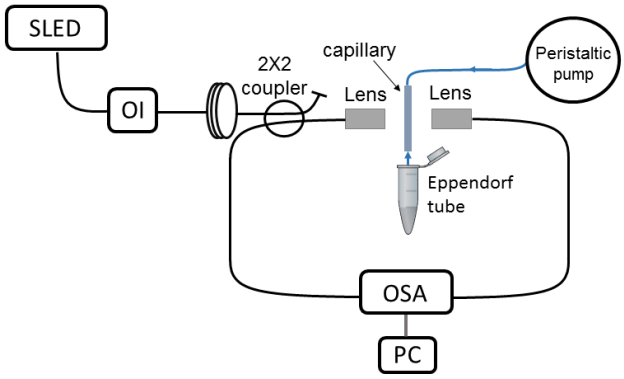

Fig. 6. Instrumental configuration for optical power measurements on glass micro-capillaries. SLED: Superluminescent Light Emitting Diode; OI: Optical Isolator; OSA: Optical Spectrum Analyzer; Lens: aspheric lens with pigtail style focuser; PC: personal computer.

A pigtail style focuser with aspheric lens (by OzOptics) was used to shine a 50-µm-diameter light spot (with orthogonal incidence) on the flat side of the micro-capillary, placed at a distance of approximately 23.5 mm, and at the same time to couple the back reflected light from the device under test toward the optical spectrum analyzer. Transmitted optical power was as well coupled in the fiber by means of a second lens placed on the opposite side of the capillary. Reflected and transmitted optical signals were fed to an optical spectrum analyzer (OSA, Agilent 86142B) allowing spectra detection with resolution bandwidth RB = 0.1 nm. Both lenses were secured on a kinematic mount for optics, to ensure the precise alignment of the beam orthogonally to the capillary, in order to maximize the reflected and transmitted signals coupled in the input and output fibers, respectively. Transmitted and reflected optical spectra were acquired from the OSA by a personal computer with a custom designed LabVIEW interface. All spectra were filtered with a third order low-pass digital Butterworth filter with $f_t = 1/\lambda = 2000$ [μm^{-1}] to improve the signal to noise ratio. Since the SLED has a Gaussian-shaped emission spectrum, the reflected spectrum was normalized to the spectrum of the optical signal incident on the capillary, whereas the transmitted spectrum was normalized with respect to a reference spectrum captured in transmission without the capillary. Data were then interpolated obtaining a wavelength step equal to 10 pm. Typical normalized spectra acquired on a capillary with nominal geometrical parameters $d = t_f = t_b$ = 50 µm filled with water are shown in Fig. 7. According to what is theoretically expected, a good correspondence between the wavelength positions of the reflectivity maxima and transmissivity minima (and vice versa) is observed. The spectral line shape obtained experimentally resembles the theoretical results reported in Fig. 2 and differences are probably due to fabrication tolerances on the effective value of the wall thicknesses.

Biomedical Optics EXPRESS

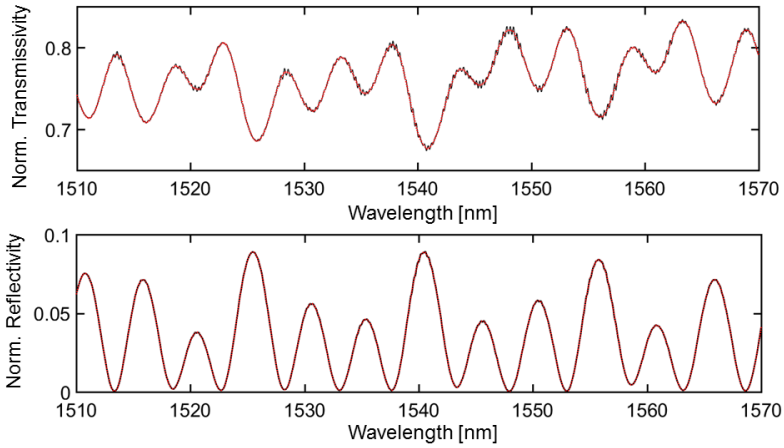

Fig. 7. Normalized optical spectra acquired on a capillary with $d = t_f = t_b = 50$ µm (nominal values). Black traces: raw data; Red traces: interpolated and filtered data. Upper traces: transmitted signal; Lower traces: reflected signal. Wavelength step (after interpolation) $1*10^{-5}$ µm.

4. Experimental results

Experimental aims of this study were to demonstrate that the spectral shift of the T/R ratio, between transmitted and reflected optical signals, depends on the refractive index of water-glucose solutions flowing through the micro-capillary, and thus can be proposed as a method for refractive index sensing in flow-through applications, as well as to compare the sensitivity obtained with capillaries featuring different combinations of channel depth and wall thickness.

4.1 Results on capillaries with channel depth d = 50 µm

Figure 8 shows the sequence of T/R spectra (T = normalized transmitted signal, R = normalized reflected signal) acquired on a capillary with channel depth $d = 50$ µm and wall thickness $t_f = t_b = 50$ µm (nominal values) when it was filled with glucose solutions in water at concentrations varying from 0% up to 11% [w/V], resulting in RI values from 1.3154 RIU to 1.3313 RIU. As the RI of the filling solution increased, a shift of the spectra maxima toward longer wavelengths was observed. Figure 9 offers a 3D representation of data, where the signal amplitude is expressed in false colors and the shift toward longer wavelengths induced by increasing RI is better visualized. Reporting the wavelength position of the maxima of the T/R spectra as a function of the solution RI, we obtained the calibration curves of the refractive index sensor (shown in Fig. 10(a)). Defining the sensitivity (S) as the spectral shift induced by a given RI variation, or $S = d\lambda_{max}/dn_{fluid}$, we observed that the peaks featured different sensitivities: for the capillary with $d = t_f = t_b = 50$ µm, the highest value was $S_{max} = (d\lambda_{max}/dn_{fluid})_{max} = 345.9$ RIU (relative to the light green trace in Fig. 10(a), the sixth from the top). Another important parameter is the limit of detection (LoD) which gives the minimum change of the variable under test that can be detected, defined as 36/S [34], where 6 is the standard deviation calculated on at least three repeated acquisitions. LoDs calculated for each T/R spectra maxima were found in the range of $5.1x10^{-5}$ and $4.5x10^{-4}$ RIU. The maximum value of $\Delta\lambda$ on the spectrum relative to pure water filling was $\Delta\lambda_{water\text{-}max} = 5.7$ nm. Data in Figs. 7, 8, 9 and 10(a) refer to the same device.

Biomedical Optics EXPRESS

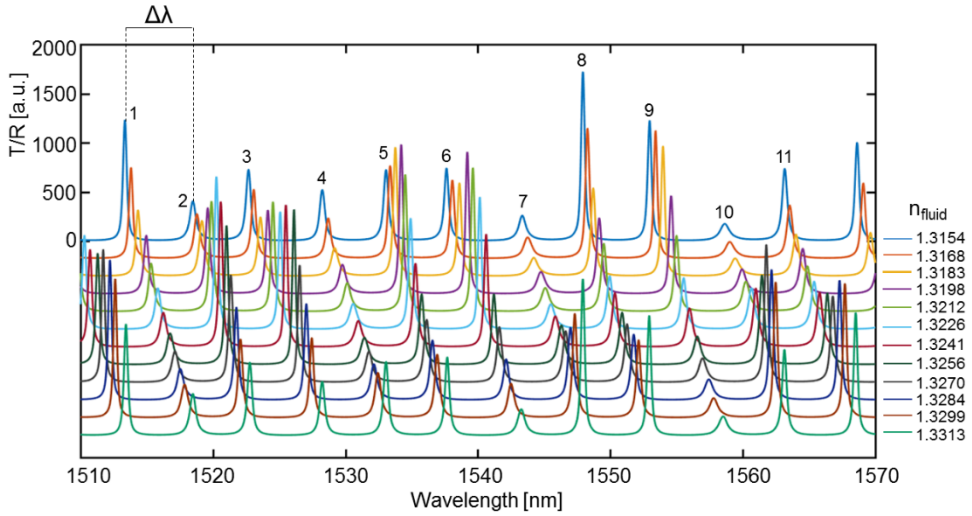

Fig. 8. T/R ratio measured on a capillary with $d = t_f = t_b = 50$ µm. Traces are relative to glucose solutions in water with RI from 1.3154 RIU (water) to 1.3313 RIU; the legend is reported on the right. Traces have been vertically shifted of −180 a.u. for a better visualization. The absolute scale, on the y-axis, refers only to the trace relative to water.

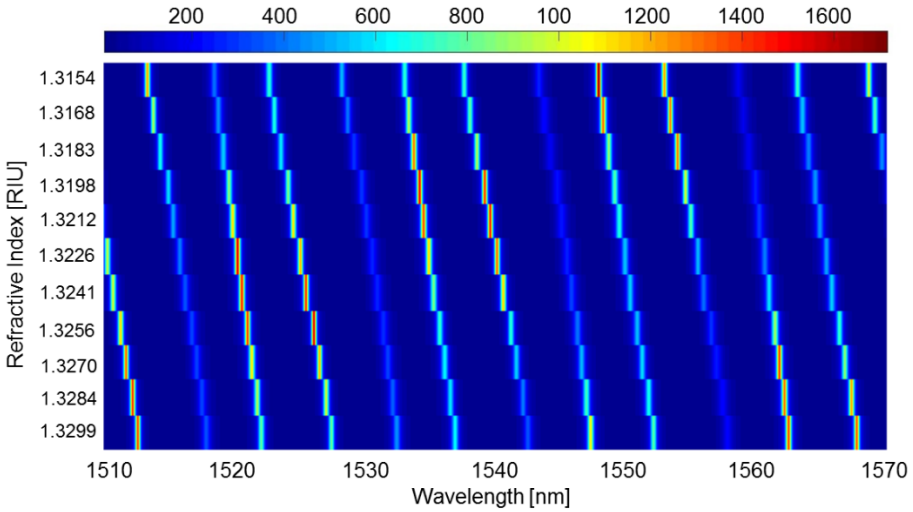

Fig. 9. 2D view of the 3D reconstruction of the T/R spectra shown in Fig. 8. Amplitude values are represented using false colors, indicated on top of the graph.

We repeated the experiments on a capillary with the same channel depth but thinner walls, thus d = 50 µm and $t_f = t_b$ = 35 µm (nominal values), to investigate the impact of these parameters on the sensitivity. The calibration curves relative to this second kind of capillary are reported in Fig. 10(b). In this case, the highest sensitivity was S_{max} = 530.9 nm/RIU (relative to the light blue trace in Fig. 10(b), the second from the bottom), thus higher than the one obtained on the capillary with the same channel depth but thicker walls, and LoD of the order of 10^{-5}-10^{-4} RIU. We also observed a $\Delta\lambda_{water\text{-}max}$ = 7.65 nm.

Biomedical Optics EXPRESS

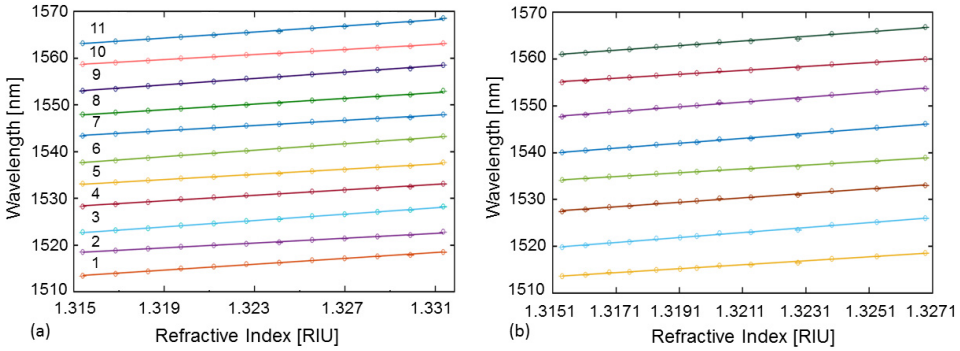

Fig. 10. Wavelength positions of T/R maxima as a function of glucose solution RI: mean values (empty circles) and standard deviations (error bars) calculated on three spectral acquisitions. Straight lines represent the best linear fitting of the data. (a) capillary with $t_f = t_b = d = 50$ µm. The numbers reported near each fitting line recall the peaks numbering highlighted in Fig. 8. (b) capillary with $t_f = t_b = 35$ µm and $d = 50$ µm (nominal values).

4.2 Results on capillary with channel depth 30 µm

We also tested a capillary with channel depth $d = 30$ µm and wall thickness $t_f = t_b = 30$ µm. Figure 11(a) shows the representation in false colors of the T/R spectra obtained on this micro-device. As a consequence of the narrower channel, a higher $\Delta\lambda_{max}$ was observed (in particular, in presence of water, the largest value was $\Delta\lambda_{water\text{-}max} = 13.2$ nm) and, consequently, less peaks of the T/R spectra were present in the wavelength range of interest. Figure 11(b) reports the calibration curves for this capillary. We obtained $S_{max} = 484.2$ nm/RIU (relative to the red trace in Fig. 11(b)), and LoD of the same order of magnitude of that found for other capillaries.

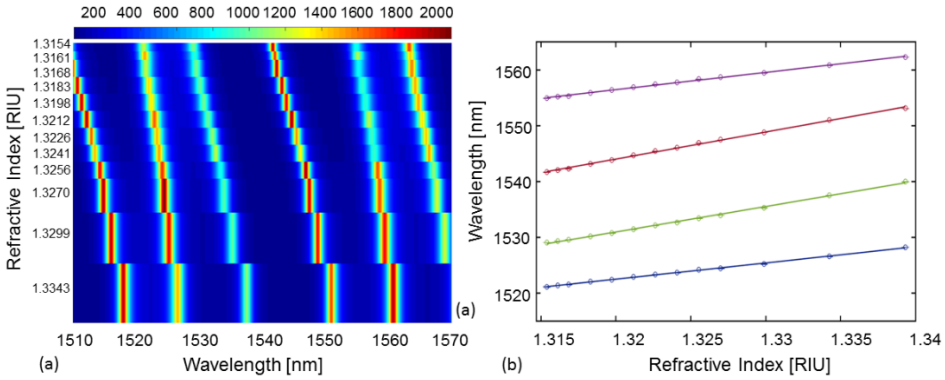

Fig. 11. (a) 2D view of the 3D reconstruction of the detected T/R spectra relative to a capillary with $d = t_f = t_b = 30$ µm. Amplitude values are represented using false colors. (b) Wavelength positions of T/R maxima as a function of glucose solution RI: mean values (empty circles) and standard deviations (error bars) calculated on three spectral acquisitions. Straight lines represent the best linear fitting of the data. Capillary with $d = t_f = t_b = 30$ µm (nominal values).

4.3 Amplitude detection at a single wavelength

In the previous sections, calibration curves were reconstructed by monitoring the shift of the T/R peaks, acquired on a 60-nm wavelength range. T/R spectra, as previously stated, are not affected by fluctuations of the read-out source optical power. This feature paves the way for performing RI measurements by detecting the T/R amplitude at a single wavelength, a method that would lead to a more compact system. In order to further investigate this development, we focused our attention to T/R amplitude changes occurring at a selected

Biomedical Optics EXPRESS

wavelength. As shown in Fig. 12(a), at λ = 1541.7 nm, as the RI of the filling media increases, the amplitude decreases, as a consequence of the spectral shift toward longer wavelengths.

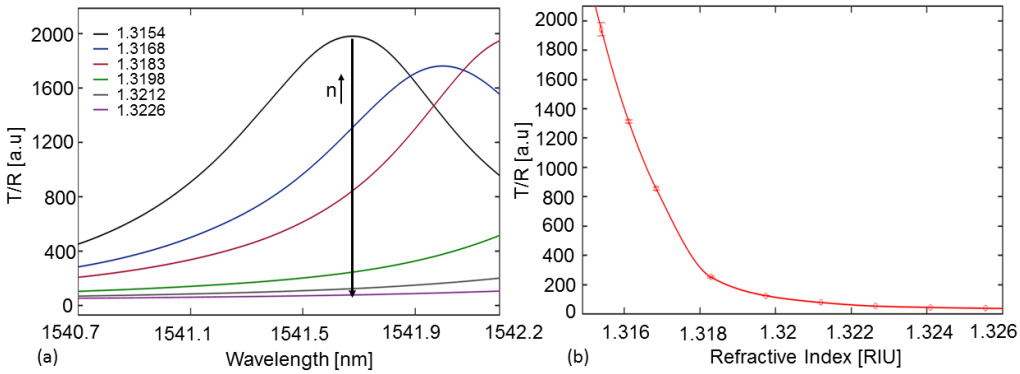

Fig. 12. (a) Zoom of the T/R spectra relative to a capillary with $d = t_f = t_b = 30$ µm on a 1.5-nm interval. Spectral amplitude at a single wavelength decreases as the glucose RI increases. (b) Mean values and standard deviations of the T/R amplitude at $\lambda = 1541.7$ nm extracted from data of Fig. 12(a) as a function of the RI. A shape-preserving interpolant curve provides data fitting.

Reporting T/R values at λ = 1541.7 nm versus fluid RI, we obtained a different kind of calibration curve, which is reported in Fig. 12(b). Two trends are observable, one with higher slope for RI from 1.3154 RIU to 1.3183 RIU, relative to glucose concentrations from 0% to 2% and one with lower slope for higher RI values. No significant changes in the spectra amplitude were observable for RI higher than 1.3256 RIU. These results suggest the possibility to measure fluid RI using a commercially available semiconductor laser emitting in the telecom wavelength range and two photodiodes to detect the transmitted and reflected power at a selected wavelength, thus obtaining a more compact and less expensive system. Measuring the amplitude of the ratio T/R has the intrinsic advantage of cancelling spurious signals variations due to input power fluctuations. Performing a linear fitting for RI values between 1.3154 and 1.3168 RIU, we obtained a sensitivity equal to 750.3×10^3 [a.u./RIU] and LoD equal to 4.76×10^{-5} RIU, calculated on the central value of the highly sensitive region.

5. Discussion

In Section 2, we have reported how the internal dimensions of the capillary theoretically affect their optical performances by means of numerical simulations of the T/R spectra. To verify the agreement between experimental and theoretical results, we measured on the tested devices the effective value of channel depth, d_{eff}, as well as of the optical path of the front glass wall, $n_{glass} \cdot t_{f,eff}$, and of the back glass wall, $n_{glass} \cdot t_{b,eff}$, by means of low-coherence reflectometry in the near-infrared, presented in our previous works [35,36]. Table 1 summarizes the values of the highest sensitivity, the widest Δλ and the specific D value for all the tested capillaries. It can be noticed that the capillary with the highest effective D provides the highest sensitivity. We also report the highest Δn detectable without ambiguity, defined as $\Delta n = \Delta\lambda_{max}/S_{max}$, where $\Delta\lambda_{max}$ and S_{max} are related to the same T/R peak. As it can be seen, the capillary featuring the greatest Δn was the one with $d = t_f = t_b = 30$ µm, yielding Δn = 0.0273 RIU. In summary, the most sensitive device resulted to be the capillary with nominal wall thickness $t_f = t_b = 35$ µm and channel depth $d = 50$ µm (and the highest specific D) while the one with the widest Δλ was the capillary with $d = t_f = t_b = 30$ µm. All capillaries provided approximately the same response in terms of LoD.

Biomedical Optics EXPRESS

Table 1. Parameters of performances of different capillaries

Capillary nominal dimensions t_f-d-t_b [μm]	Highest sensitivity [nm/RIU]	Measured specific D	Widest Δλ [nm]	Highest $\Delta n = \Delta\lambda_{max}/S_{max}$ [RIU]
50-50-50	345.9	0.22	5.7	0.0165
35-50-35	530.9	0.33	7.7	0.0143
30-30-30	484.2	0.31	13.2	0.0273

6. Conclusions

In this paper, we have demonstrated the realization of a bio-chemical sensor for fluid RI detection using, as core elements, glass micro-capillaries with rectangular cross-section, integrated in a simple micro-fluidic system. Rectangular glass micro-capillaries are off-the-shelf disposable devices well suited for the optical readout, thanks to their flat surface. Their internal micrometric dimension allows to work with ultra-low quantities of material, important factor in the field of biological and clinical analysis. The transduction method of the proposed system is based on the detection of the wavelength shift of T/R maxima, exploited by means of a broadband light source emitting in the near-infrared wavelength region where the invasiveness for biological tissues is minimum. We investigated two capillaries with channel depth of 50 μm, one with walls of the same thickness and one with 35-μm-thick walls, as well as one with channel depth and wall thickness of 30 μm. We tested the devices with solutions of glucose in water at increasing concentrations and obtained LoD in the range of 10^{5}-10^{-4} RIU and sensitivities higher than 258.0 nm/RIU, with a maximum value of 530.9 nm/RIU, obtained for the capillary with $t_f = t_b = 35$ μm and $d = 50$ μm. These sensitivity values are comparable with those found in the literature but often obtained with devices fabricated or custom modified by means of sophisticated micromachining techniques. Moreover, we noticed that the sensitivity is related to the ratio of the channel depth to the overall optical path length. The possibility of collecting both reflected and transmitted optical power is an interesting feature of transparent devices like the glass micro-capillary, since the estimation of the ratio between transmitted and reflected spectra eliminates the need of an external monitoring system for the emitted optical power in amplitude-based sensors. On the other side, this work lacks demonstration of surface sensitivity and specificity: however, it has been proved that non-specific refractometric measurements can be suitable to accurately detect glucose concentration if associated with different measuring techniques, like for example electrical conductivity measurements [37].

Future development will be devoted to apply these devices for demonstrating surface sensitivity and to the realization of measurements at a single wavelength, using a commercially available semiconductor laser in the telecom range as read-out source and two photodiodes for the detection of the transmitted and reflected optical power, thus allowing to realize a more compact and portable system, where no OSA or other optical filtering components will be necessary.

Appendix

Model for numerical calculation of the spectral reflectivity and transmissivity

The capillary can be considered as a multilayer structure composed by alternating dielectric materials with different refractive indices and thicknesses along a single axis (one-dimensional structure), since the beam diameter is always smaller than the width/length of the flat side of the capillary. Even though the reflectivity of this kind of structures is often calculated by transfer matrix methods, which can be eventually generalized for two- and three-dimensional structures, we selected an approach based on electromagnetic field propagation for the sake of simplicity since we are only interested in describing a one-

Biomedical Optics EXPRESS

dimensional structure composed by three different layers immersed in air. This approach considers the electric field propagation across the capillary modeled as a cascade of Fabry-Perot etalons, as shown in Fig. 13.

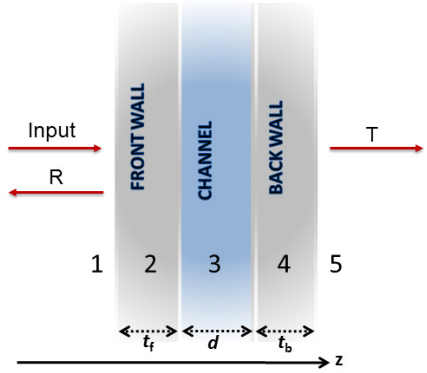

Fig. 13. Schema of the capillary interfaces, used for numerical simulations.

Starting by considering the layer of the back glass-wall of the capillary, we can identify two interfaces: 3-4 between channel (3) and back glass-wall (4) and 4-5 between back glass-wall (4) and air (5). We assume that t_b is the thickness of the back wall, n_{glass} is the refractive index of glass, n is the refractive index of the fluid in the channel and $n_{air} = 1$. We also assume a plane wave propagating in the z-direction perpendicular to the interfaces. If we define the field reflection (ρ) and transmission (τ) coefficients for the wave propagating through the interfaces as:

$$\rho_{3-4} = \left(n - n_{glass}\right) / \left(n + n_{glass}\right) = -\rho_{4-3}$$

$$\rho_{4-5} = \left(n_{glass} - n_{air}\right) / \left(n_{glass} + n_{air}\right) = \left(n_{glass} - 1\right) / \left(n_{glass} + 1\right)$$

$$\tau_{3-4} = 2n / \left(n + n_{glass}\right)$$

$$\tau_{4-3} = 2n_{glass} / \left(n_{glass} + n\right)$$

$$\tau_{4-5} = 2n_{glass} / \left(n_{glass} + 1\right),$$

then, the electric field reflection coefficient $\rho_{3\text{-}4'}$ of the whole back glass-wall, considered as an overall equivalent interface 3-4', can be calculated as:

$$\rho_{3-4'} = \rho_{3-4} + \frac{\tau_{3-4}\tau_{4-3}\rho_{4-5}e^{\left(-j2kn_{glass}t_b\right)}}{1 - \rho_{4-3}\rho_{4-5}e^{\left(-j2kn_{glass}t_b\right)}}$$

and the electric field transmission coefficient $\tau_{3\text{-}4'}$ of the whole back glass-wall can be calculated as:

$$\tau_{3-4'} = \frac{\tau_{3-4}\tau_{4-5}e^{\left(-jkn_{glass}t_b\right)}}{1 - \rho_{4-3}\rho_{4-5}e^{\left(-j2kn_{glass}t_b\right)}}$$

where $k = 2\,\pi / \lambda$.

By iteratively computing the electric field reflection coefficient in the backward direction with respect to the incident wave, the reflectivity of the capillary can be calculated. By considering the layer of the capillary channel, we can now identify two interfaces: 2-3

Biomedical Optics EXPRESS

between front glass-wall (2) and channel (3) and 3-4' between channel (3) and equivalent medium 4'. We assume here that d is the channel depth. The electric field reflection coefficient $\rho_{2\text{-}3'}$ at the overall equivalent interface 2-3′ is given by:

$$\rho_{2-3'} = \rho_{2-3} + \frac{\tau_{2-3}\tau_{3-2}\rho_{3-4'}e^{(-j2knd)}}{1-\rho_{3-2}\rho_{3-4'}e^{(-j2knd)}}$$

and the electric field transmission coefficient $\tau_{2\text{-}3'}$ is given by:

$$\tau_{2-3'} = \frac{\tau_{2-3}\tau_{3-4'}e^{(-jkd)}}{1-\rho_{3-2}\rho_{3-4'}e^{(-j2kd)}}$$

where

$$\rho_{2-3} = \left(n_{\text{glass}} - n\right) / \left(n_{\text{glass}} + n\right) = -\rho_{3-2}$$

$$\tau_{2-3} = 2n_{\text{glass}} / \left(n_{\text{glass}} + n\right)$$

$$\tau_{3-2} = 2n / \left(n + n_{\text{glass}}\right).$$

Finally, assuming that t_f is the thickness of the front wall, in analogy with the previous steps, the electric field reflection coefficient of the whole capillary $\rho_{1\text{-}2'}$ is given by:

$$\rho_{1-2'} = \rho_{1-2} + \frac{\tau_{1-2}\tau_{2-1}\rho_{2-3'}e^{(-j2kn_{glass}t_f)}}{1-\rho_{2-1}\rho_{2-3'}e^{(-j2kn_{glass}t_f)}}$$

and the electric field transmission coefficient of the whole capillary $\tau_{1\text{-}2'}$ is given by:

$$\tau_{1-2'} = \frac{\tau_{1-2}\tau_{2-3'}e^{(-jkn_{glass}t_f)}}{1-\rho_{2-1}\rho_{2-3'}e^{(-j2kn_{glass}t_f)}}$$

where

$$\rho_{1-2} = \left(1 - n_{\text{glass}}\right) / \left(1 + n_{\text{glass}}\right) = -\rho_{2-1},$$

$$\tau_{1-2} = 2 / \left(1 + n_{\text{glass}}\right),$$

$$\tau_{2-1} = 2n_{\text{glass}} / \left(n_{\text{glass}} + 1\right).$$

The spectral reflectivity R is then obtained by plotting $|\rho_{1\text{-}2'}|^2$ as a function of the wavelength λ whereas the spectral transmissivity T is obtained by plotting $|\tau_{1\text{-}2'}|^2$ as a function of the wavelength λ.

Acknowledgments

The authors wish to thank VitroCom for providing glass capillary samples.

Disclosures

The authors declare that there are no conflicts of interest related to this article.